The Astrophysical Journal, 871:162 (10pp), 2019 February 1 https://doi.org/10.3847/1538-4357/aaf6e4

Optical Spectroscopic Survey of a Sample of Unidentified *Fermi* Objects: II

Simona Paiano[1,2], Renato Falomo[1], Aldo Treves[3,4], Alberto Franceschini[5], and Riccardo Scarpa[6,7]
[1] INAF, Osservatorio Astronomico di Padova, Vicolo dell'Osservatorio 5 I-35122 Padova, Italy; simona.paiano@inaf.it
[2] INFN, Sezione di Padova, via Marzolo 8, I-35131 Padova, Italy
[3] Università degli Studi dell'Insubria, Via Valleggio 11 I-22100 Como, Italy
[4] INAF, Osservatorio Astronomico di Brera, Via E. Bianchi 46 I-23807 Merate (Lecco), Italy
[5] Dipartimento di Fisica e Astronomia, Università di Padova, Vicolo dell'Osservatorio 3, I-35 Padova, Italy
[6] Instituto de Astrofisica de Canarias, C/O Via Lactea, s/n E38205—La Laguna (Tenerife), Spain
[7] Universidad de La Laguna, Dpto. Astrofsica, s/n E-38206 La Laguna (Tenerife), Spain
Received 2018 October 8; revised 2018 November 8; accepted 2018 November 20; published 2019 January 29

Abstract

We report on optical spectroscopy obtained at the 10.4 m Gran Telescopio Canarias of 28 *Fermi* γ-ray sources that completes the study of a sample of 60 targets of unidentified objects for which the detection of an X-ray and/or radio source inside the 3FGL error box is available. The observations aim to characterize the nature and measure the redshift of these sources. For all optical counterparts, the observations allow us to establish their active galactic nucleus nature. In particular, we found 24 BL Lac objects, one quasar, one narrow line Seyfert 1, and two objects showing spectral features typical of Seyfert 2 galaxies. For most of these, we determine a spectroscopic redshift, while for five we can set lower limits based on the lack of stellar features from the host galaxy. The global properties of the full sample are briefly discussed.

Key words: BL Lacertae objects: general – galaxies: distances and redshifts – gamma rays: galaxies – techniques: spectroscopic

Supporting material: data behind figure, figure sets

1. Introduction

The population of jetted active galactic nuclei (AGNs) known as blazars are characterized by extreme properties explained by the flux amplification from relativistic bulk motions of the non-thermal emitting plasma inside the jet oriented at a small angle with respect to the line of sight of the observer. A consequence of this is their huge photon emissivity at high, up to very high, photon energies (>100 MeV), interpreted as inverse Compton or even photohadronic processes.

From the optical spectroscopic point of view, blazars are divided in two sub-classes: BL Lac objects (BLLs) and Flat Spectrum Radio Quasars (FSRQs), depending on the strength of the broad emission lines with respect to the continuum; the latter display strong and broad emission lines, while the former are characterized by optical spectra featureless or with very weak emission/absorption lines (see, e.g., the review of Falomo et al. 2014).

The *Fermi* observatory, which has produced an all-sky survey at such high energies (Atwood et al. 2009), is then ideally suited to detect blazars in large numbers. In the release of the *Fermi* survey catalog (3FGL; Acero et al. 2015), reporting 3033 detected γ-ray emitters, and in the third *Fermi* catalog of high-energy sources (3FHL; The Fermi-LAT Collaboration 2017), more than one thousand of them are already indicated as blazars or blazar candidates, resulting in being the dominant population of the extragalactic high-energy sky.

On the other hand, because of the *Fermi* angular resolution (the median error box radius is ∼5 arcmin in the 3FGL catalog), about one third of the 3FGL sources are still unassociated to counterparts in other frequency bands (the unassociated/unidentified gamma-ray sources, henceforth UGSs). This is due either to the lack of observations at other wavelengths, especially in the X-ray band, or to the presence of many possible counterparts in their γ-ray error box. The UGS population then not only represents a fundamental component of the high-energy sky, but is also hiding a substantial fraction of the whole blazar population (Massaro et al. 2012; Mirabal et al. 2012; Acero et al. 2013; D'Abrusco et al. 2013; Doert & Errando 2014; Landi et al. 2015; Paiano et al. 2017a). It is then of utmost interest to perform a full investigation of these sources in order to find their astrophysical counterparts. In particular, it is of key importance to obtain spectroscopy of the optical counterparts in order to assess their classification and to determine the redshift. Since the population of UGSs is expected to be dominated by objects of BLL-type that are characterized by very weak spectral features, the use of large telescopes is mandatory (see, e.g., Paiano et al. 2017c and references therein).

In Paiano et al. (2017a), hereafter Paper I, we defined a sample of 60 UGSs selected from the 2FGL and 3FGL catalogs and with at least one X-ray source detected inside the UGS error box. In the case where more than one X-ray source appears within the *Fermi* error box, we select that coincident with a radio source. Once the X-ray counterpart is fixed, the association process then consists in searching for counterparts of the X-ray source at radio, infrared (IR), and optical frequencies (see the details and example in Figure 1 of Paper I). At variance with the above procedure, in two cases no X-ray counterpart is available, but one/two radio sources are present. For these targets, we consider the likely counterpart of the gamma-ray source, only the one that also has a counterpart both at optical and IR bands.

In Paper I, we presented optical spectroscopy of 20 targets which allowed us to provide the source classification and to derive their redshift. In this work, following the same association strategy of Paper I, we report on spectra of the optical counterparts for another 28 UGSs (see Table 1). The spectroscopic study is thus complete for 80% of sources of the sample. With this new effort, we set out the basis to start identifying interesting trends in the redshift distributions of the different blazar categories, in particular for the BLLs versus FSRQs, which have been the subject of a

Table 1
The Sample

3FGL Name	Optical Counterpart	R.A. (J2000)	Decl. (J2000)	3FHL	mag	$E(B-V)$	z	Reference
3FGLJ0004.2+0843	SDSSJ000359+084138	00:03:59.23	+08:41:38.2	n	20.2	0.0614	2.06-0.19?	SDSS
3FGLJ0006.2+0135	SDSSJ000626+013610	00:06:26.92	+01:36:10.3	n	20.3	0.0264	?	
3FGLJ0031.6+0938	SDSSJ003159+093618	00:31:59.86	+09:36:18.4	n	19.5	0.0505	?	
3FGLJ0158.6+0102	SDSSJ015852+010132	01:58:52.77	+01:01:32.8	n	21.1	0.0225	0.952?	SDSS
3FGLJ0234.2-0629	SDSSJ023410-062825	02:34:10.27	−06:28:25.6	n	20.5	0.0225	?	SDSS
3FGLJ0251.1-1829	USNOB1-0714-0029276	02:51:11.55	−18:31:14.3	y	19.5	0.0237	?	
3FGLJ0258.9+0552	SDSSJ025857+055243	02:58:57.55	+05:52:43.9	y	18.9	0.1196	?	
3FGLJ0414.9-0840	USNOB1-0812-0041101	04:14:33.08	−08:42:06.7	n	19.3	0.0405	?	
3FGLJ0506.9+0321	USNOB1-0933-0085213	05:06:50.14	+03:23:58.6	y	18.4	0.0593	?	
3FGLJ0848.5+7018	USNOB1-1602-0082223	08:48:39.52	+70:17:28.0	y	19.7	0.0274	?	
3FGLJ0930.7+5133	SDSSJ093033+513214	09:30:33.36	+51:32:14.6	n	20.0	0.0149	?	
3FGLJ1146.1-0640	USNOB1-0833-0250645	11:46:00.96	−06:38:54.8	y	19.7	0.0285	?	
3FGLJ1223.3+0818	SDSSJ122327+082030	12:23:27.49	+08:20:30.4	n	19.8	0.0199	?	
3FGLJ1234.7-0437	USNOB1-0854-0232216	12:34:48.00	−04:32:46.2	y	19.8	0.0322	0.277	NED
3FGLJ1258.4+2123	SDSSJ125821+212351	12:58:21.45	+21:23:51.0	n	20.6	0.0342	?	
3FGLJ1525.8-0834	USNOB1-0814-0287412	15:26:03.17	−08:31:46.4	n	18.8	0.0796	?	
3FGLJ1541.6+1414	SDSSJ154150+141437	15:41:50.16	+14:14:37.6	y	17.2	0.0407	0.2230	SDSS
3FGLJ2150.5-1754	USNOB1-0721-1160290	21:50:46.43	−17:49:54.5	n	18.2	0.0435	?	
3FGLJ2209.8-0450	SDSSJ220941-045110	22:09:41.70	−04:51:10.3	y	18.8	0.0613	?	
3FGLJ2212.5+0703	SDSSJ221230+070652	22:12:30.98	+07:06:52.5	n	19.9	0.0642	?	
3FGLJ2228.5-1636	USNOB1-0733-0885778	22:28:30.18	−16:36:43.0	n	18.7	0.0295	?	
3FGLJ2229.1+2255	SDSSJ222911+225459	22:29:11.18	+22:54:59.9	n	18.9	0.0455	?	
3FGLJ2244.6+2503	SDSSJ224436+250342	22:44:36.70	+25:03:42.6	n	19.3	0.0573	?	
3FGLJ2246.2+1547[a]	SDSSJ224604+154435	22:46:04.90	+15:44:35.5	y	19.3	0.0673	?	Paiano et al. (2017a)
3FGLJ2250.3+1747	SDSSJ225032+174914	22:50:32.88	+17:49:14.8	n	19.9	0.0675	?	
3FGLJ2321.6-1619	USNOB1-0736-0835813	23:21:37.01	−16:19:28.5	n	17.9	0.0239	?	
3FGLJ2358.6-1809	USNOB1-0718-1032041	23:58:36.72	−18:07:17.4	y	17.45	0.0214	0.0575?	NED
3FGLJ2358.5+3827	USNOB1-1284-0547072	23:58:25.17	+38:28:56.4	y	19.0	0.1051	?	

Note. Column 1: name of the target; Column 2: optical counterpart of the target; Columns 3, 4: R.A. and decl. of the optical counterpart; Column 5: source reported in the 3FHL catalog; Column 6: g magnitude from the SDSS (for the SDSS sources) or B-band magnitudes taken from USNOB1.0 catalog; Column 7: $E(B-V)$ taken from the NASA/IPAC Infrared Science Archive (https://irsa.ipac.caltech.edu/applications/DUST/); Column 8: redshift reported in the literature; Column 9: reference for the redshift.
[a] This source was also discussed in Paper I.

long debate (e.g., Padovani et al. 2017; Garofalo et al. 2018). In Section 2, we present the observations and data reduction. In Section 3, we summarize our results and report on the new redshifts. Section 4 is devoted to detailed notes for individual sources, and in Section 5 we outline our main conclusions.

2. Observations and Data Reduction

The observations were carried out in service mode between 2016 September and 2018 January using the spectrograph OSIRIS (Cepa et al. 2003) at the 10.4 m Gran Telescopio Canarias (GTC) (see Table 2). The instrument was configured with the grism R1000B, covering the spectral range 4100–7500 Å, and a slit width of 1.″2. The strategy of the observations and the data reduction are the same as described in the Paper I and for each source at least three individual exposures were obtained in order to remove cosmic rays and CCD cosmetic defects. All exposures were combined into a single average image. Wavelength calibration was performed using the spectra of Hg, Ar, Ne, and Xe lamps. Spectra were corrected for atmospheric extinction using the mean La Palma site extinction. For each source, during the same observation night, we observed a spectro-photometric standard star in order to perform the relative flux calibration. Also an absolute flux calibration was done using the source magnitude (reported in Table 2) estimated by a direct g filter image obtained as part of the target acquisition. No significant magnitude variations with respect to the literature values were found (compare Tables 1 and 2). Finally each spectrum was dereddened for the Galaxy contribution, applying the extinction law by Cardelli et al. (1989) and assuming the $E(B-V)$ values taken from the NASA/IPAC Infrared Science Archive 6.

3. Results

Optical images of the UGSs are displayed in Figure 1 together with the error box of the X-ray and radio counterparts (if available). In Figure 2, we show the flux-calibrated and dereddened optical spectra[8] of the counterparts of 28 3FGL γ-ray emitters. To emphasize weak emission and/or absorption features, we display also the normalized spectra, obtained dividing the spectrum by its continuum (see the details in Paper I). From each normalized spectrum, we evaluated the signal-to-noise ratio (S/N) value in a number of spectral regions (see Table 3). All spectra were carefully inspected to find emission and/or absorption lines. We checked their reliability by comparing the features in individual exposures (see Section 2 for details).

For most of the targets (23 out of 28), we clearly found spectral lines (see Tables 3 and 4). In Figure 3, we report close-ups of the spectra showing the faintest detected spectral lines.

[8] All spectra are also available at the online ZBLLAC database: http://www.oapd.inaf.it/zbllac/.

Table 2
Log of the Observations

Obejct	Obs. Date	t_{Exp} (s)	Seeing ($''$)	g
3FGLJ0004.2+0843	2016 Oct 05	3600	1.3	20.2
3FGLJ0006.2+0135	2016 Oct 06	7200	2.5	20.3
3FGLJ0031.6+0938	2017 Dec 03	3600	1.6	19.2
3FGLJ0158.6+0102	2016 Sep 25	8750	1.5	21.4
3FGLJ0234.2-0629	2016 Oct 05	10,200	2.5	19.7
3FGLJ0251.1-1829	2017 Sep 26	2000	1.3	19.1
3FGLJ0258.9+0552	2016 Sep 15	3600	1.5	19.2
3FGLJ0414.9-0840	2016 Sep 16	9000	2.0	19.2
3FGLJ0506.9+0321	2016 Sep 15	1500	1.3	18.8
3FGLJ0848.5+7018	2016 Dec 10	5100	1.9	19.9
3FGLJ0930.7+5133	2018 Jan 27	6000	1.3	20.1
3FGLJ1146.1-0640	2016 Dec 29	15,000	1.8	19.3
3FGLJ1223.3+0818	2017 Mar 24	7500	1.5	18.9
3FGLJ1234.7-0437	2017 Apr 12	7500	3.0	18.6
3FGLJ1258.4+2123	2017 Apr 03	7500	1.6	20.5
3FGLJ1525.8-0834	2017 Apr 02	3000	1.8	18.3
3FGLJ1541.6+1414	2017 Apr 13	1500	0.8	18.4
3FGLJ2150.5-1754	2017 Dec 08	1800	2.5	17.6
3FGLJ2209.8-0450	2017 Sep 22	3000	1.6	18.8
3FGLJ2212.5+0703	2017 Sep 26	2400	0.9	20.6
3FGLJ2228.5-1636	2017 Jun 22	2500	1.2	18.8
3FGLJ2229.1+2255	2017 Sep 29	3000	0.9	18.9
3FGLJ2244.6+2503	2017 Jun 22	8500	1.3	18.9
3FGLJ2246.2+1547	2017 Aug 11	7200	0.9	19.1
3FGLJ2250.3+1747	2017 Sep 20	3600	1.8	20.2
3FGLJ2321.6-1619	2017 Sep 26	7200	1.1	16.9
3FGLJ2358.6-1809	2017 Sep 29	9000	2.0	17.7
3FGLJ2358.5+3827	2017 Sep 24	4500	2.0	18.4

Note. Column 1: name of the target; Column 2: date of observation; Column 3: total integration time; Column 4: seeing during the observation; Column 5: g magnitude measured from the acquisition image.

In the case of 15 objects we detect absorption lines due to the host galaxies (e.g., Ca II 3934, 3968 Å, G-band 4305 Å, Mg I 5175 Å, and Na I 5893 Å), and for 10 sources we have emission lines, mainly [O II] 3727 Å and [O III] 5007 Å. For seven targets both stellar absorptions and emission lines are detected. In spectra of 10 objects we have not revealed intrinsic emission/absorption features. However for half of them we detected intervening absorption systems of Mg II 2800 Å that enable us to set a spectroscopic lower limit of the redshift. For the remaining five targets, the optical spectra are featureless. For these sources, assuming that all BLLs are hosted by a massive elliptical galaxy and from the non-detection of the spectral absorption features of the host galaxies (Paiano et al. 2017b), we set a redshift lower limit based on the estimate of the minimum equivalent width (EW) (see also Table 3).

From these spectroscopic observations, we classify 24 targets as BLLs, one object (3FGL J2212.5+0703) is a quasi-stellar object (QSO), and another (3FGL J0031.6+0938) is a narrow line Seyfert 1 (NLSy1) (see the details in Section 4). Finally two sources (3FGLJ1234.7-0437 and 3FGLJ2358.5 +3827) show a spectrum that exhibits prominent and narrow emission lines of [O II] 3727 Å, H_β, and [O III] 5007 Å, typical of Seyfert 2 galaxies.

4. Notes on Individual Sources

3FGL J0004.2+0843. In the 3FGL sky region of this source, we found only one object emitting at 1.4 GHz (NVSS J000359+084137). This coincides with the $g = 20.2$ optical counterpart SDSS J000359+084138. The SDSS spectrum appears featureless, although the automatic procedure proposed two tentative values of redshift ($z = 2.057$ and $z = 0.187$).

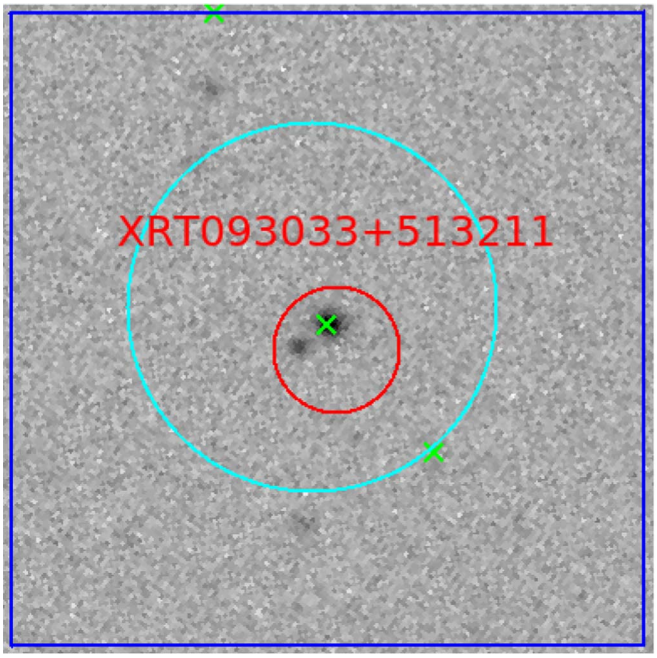

Figure 1. Optical images of the proposed counterparts of the γ-ray sources. The images are taken from the SDSS (g filter) or DSS survey (B filter), field = 60 arcsec × 60 arcsec, north up, east left. Details of the optical counterparts are reported in Table 1. The red circles represent the error box of the proposed X-ray counterparts of the γ-ray sources found with *Swift*/XRT data (magenta circles indicate an X-ray source of the *ROSAT* catalog), the cyan circles the radio counterparts (see the details in Section 1), and the green crosses the *WISE* IR counterparts. The optical image of 3FGLJ2246.2+1547 is displayed in Paper I.
(The complete figure set (27 images) is available.)

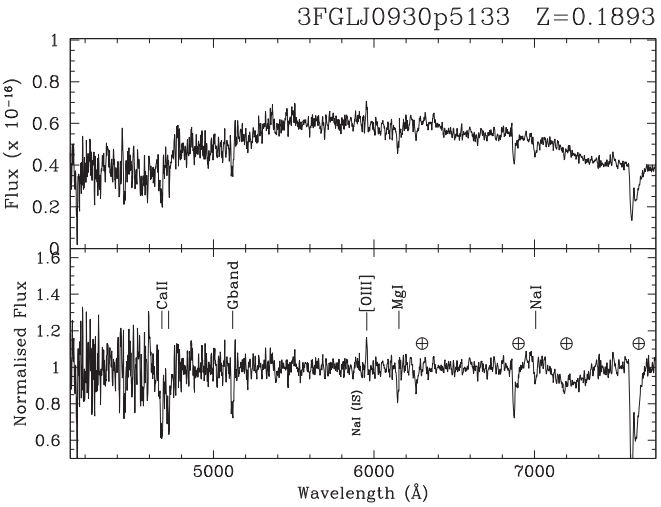

Figure 2. Spectra of the UGSs obtained at the GTC. Top panel: flux calibrated and dereddened spectra. Bottom panel: normalized spectra. The main telluric bands are indicated by ⊕, the absorption features from the interstellar medium of our galaxies are labeled as IS (Inter-Stellar). The data used to create this figure are available.
(The complete figure set (28 images) is available.)

Table 3
Properties of the Optical Spectra

OBJECT	α	S/N	EW_{min}	Class	z
3FGLJ0004.2+0843	−0.95	50	0.40–0.80	BLL	>1.5035 (a)
3FGLJ0006.2+0135	−0.90	35	0.75–1.05	BLL	0.787 (g)
3FGLJ0031.6+0938	−1.90	30	0.55–1.85	NLSY1	0.2207 (e)
3FGLJ0158.6+0102	−1.00	15	2.2–3.5	BLL	0.4537 (e)
3FGLJ0234.2-0629	−1.25	90	0.35–0.50	BLL	>0.63 (a)
3FGLJ0251.1-1829	−1.05	30	0.85–1.70	BLL	>0.615 (a)
3FGLJ0258.9+0552	−1.45	150	0.20–0.40	BLL	>0.7 (h)
3FGLJ0414.9-0840	−0.70	40	0.70–1.70	BLL	>0.35 (h)
3FGLJ0506.9+0321	−1.15	30	0.80–2.80	BLL	>0.1 (h)
3FGLJ0848.5+7018	−1.10	45	0.50–0.75	BLL	>1.2435 (a)*
3FGLJ0930.7+5133	*	30	0.80–3.00	BLL	0.1893 (e), (g)
3FGLJ1146.1-0640	−0.25	40	0.75–1.05	BLL	0.6407 (g)
3FGLJ1223.3+0818	−1.15	135	0.20–0.30	BLL	>0.7187 (a)
3FGLJ1234.7-0437	−0.40	30	1.25–3.75	Sy2	0.2765 (e), (g)
3FGLJ1258.4+2123	−0.40	40	0.65–0.80	BLL	0.6265 (g)
3FGLJ1525.8-0834	−0.85	105	0.25–0.30	BLL	>0.40 (h)
3FGLJ1541.6+1414	−0.60	60	0.45–0.70	BLL	0.223 (e), (g)
3FGLJ2150.5-1754	*	50	0.55–1.25	BLL	0.1855 (g)
3FGLJ2209.8-0450	−0.80	75	0.40–0.65	BLL	0.3967 (e), (g)
3FGLJ2212.5+0703	−1.15	15	1.35–1.90	QSO	1.00 (e):
3FGLJ2228.5-1636	−0.90	55	0.50–1.10	BLL	∼0.525 (g):
3FGLJ2229.1+2255	−1.30	80	0.35–0.40	BLL	0.440 (g)
3FGLJ2244.6+2503	−1.05	160	0.20–0.25	BLL	0.650 (g):
3FGLJ2246.2+1547	−0.80	60	0.45–1.50	BLL	0.5965 (e), (g)
3FGLJ2250.3+1747	*	25	1.30–2.25	BLL	0.3437 (e), (g)
3FGLJ2321.6-1619	−1.15	135	0.20–0.35	BLL	0.6938 (g)
3FGLJ2358.6-1809	−1.40	130	0.20–0.35	BLL	>0.25 (h)
3FGLJ2358.5+3827	*	80	0.40–0.75	Sy2	0.2001 (e), (g)

Note. Column 1: name of the target; Column 2: optical spectral index derived from a power-law fit of the continuum (the spectral index is estimated only for the sources that exhibit an optical spectrum dominated by the non-thermal emission); Column 3: averaged S/N of the spectrum; Column 4: range of the minimum equivalent width (EW_{min}) derived from different regions of the spectrum; Column 5: classification derived by our optical spectrum; Column 6: spectroscopic redshift. The superscript letters are: e = emission line, g = galaxy absorption line, a = intervening absorption assuming Mg II 2800 Å identification, h = lower limit derived on the lack of detection of host galaxy absorption lines assuming a BLL elliptical host galaxy with $M(R) = -22.9$ (see the details in Paiano et al. 2017b).
(:) This marker indicates that the redshift is tentative.
(*) For this source we found other two absorption line systems due to Fe II (2382, 2600) (see the text for details).

In our spectrum, no significant emission or absorption features are found at the redshifts proposed by the SDSS. The spectrum is featureless up to 6800 Å. An absorption doublet at ∼7000 Å is detected which we identified as an intervening system due to Mg II 2800 Å (see Figures 2 and 3). This sets a spectroscopic redshift lower limit of the source at $z > 1.5035$. This is the highest redshift of our UGS sample.

3FGL J0006.2+0135. For this UGS of the 3FGL catalog, we propose the RASS source 1RXS J000626.6+01360 as an X-ray counterpart (see Figure 1), positionally coincident with the radio source NVSS J000626+013611 and in the optical SDSS J000626.92+013610.3.

Our spectrum is dominated by the typical non-thermal power-law continuum, characteristic of BLLs, and we detect an absorption doublet at 7030 and 7092 Å which we attribute to Ca II 3934, 3968 Å absorption of the host galaxy at $z = 0.787$. This detection is sound since it occurs in the clean spectral region between two atmospheric absorption bands. This source was also observed by the SDSS and appears in the DR14 release where two weak features, consistent with our detection, are present.

3FGL J0031.6+0938. Inside the *Fermi* error box of this UGS, we detect the X-ray source XRT J003159+093615, coincident with the UV source GALEXASC J003159.86 +093618.7 and the optical object SDSS J003159.85 +093618.4 of magnitude $g = 19.2$. No radio counterpart is found and no information on previous optical spectra is available in the literature.

Our spectrum clearly shows prominent emission lines (H_β and [O III] 5007 Å), typical of a Seyfert QSO, at $z = 0.2207$ (see Figure 2). We note that H_β includes also a broad component and based on the width of this line (FWHM $\sim 1300\,km\,s^{-1}$) and on the line ratio ($[O\,III]\,5007/H_\beta$) ~ 0.8 (see e.g., Komossa 2008), we propose this source be classified as an NLSy 1.

3FGL J0158.6+0102. The optical source SDSS J015852.77 +010132.8 is coincident with the X-ray source XRTJ015852 +010129 and the radio source NVSS J015852+010133, found inside the positional error box of this unassociated γ-ray emitter. The SDSS survey provides an optical spectrum showing one emission line around 7275 Å, attributed to [O II] 3727 Å, yielding $z = 0.952$ (using the automatic procedure). However, a visual inspection of the spectrum does not reveal any other plausible features corresponding to the proposed redshift. Based on the same SDSS spectrum, Massaro et al. (2014) suggested a higher value of the redshift ($z = 1.61$), but no line identification was provided.

Table 4
Measurements of the Spectral Lines

Object name	λ	EW	Line ID	z
3FGLJ0004.2+0843	7000	0.9	Mg II 2796 Å	>1.5035
	7016	0.5	Mg II 2803 Å	>1.5035
3FGLJ0006.2+0135	7030	3.1	Ca II 3934 Å	0.787
	7092	3.3	Ca II 3968 Å	0.787
3FGLJ0031.6+0938	4549	1.7	[O II] 3727 Å	0.2207
	4723	3.9	[Ne III] 3869 Å	0.2207
	4846	3.1	H_ϵ 3970 Å	0.2207
	5007	6.7	H_δ 4102 Å	0.2207
	5298	19.6	H_γ 4340 Å	0.2207
	5934	64.8	H_β 4861 Å	0.2207
	6053	13.5	[O III] 4959 Å	0.2207
	6112	36.8	[O III] 5007 Å	0.2207
	7172	5.0	He I 5876 Å	0.2207
3FGLJ0158.6+0102	7213[a]	3.5	[O III] 4959 Å	0.454
	7278	7.9	[O III] 5007 Å	0.4537
3FGLJ0234.2-0629	4564	6.9	Mg II 2800 Å	>0.63
3FGLJ0251.1-1829	4522	3.5	Mg II 2800 Å	>0.615
3FGLJ0848.5+7018	5344	2.2	Fe II 2382 Å	>1.2435
	5833	2.1	Fe II 2600 Å	>1.2435
	6273	6.0	Mg II 2796 Å	>1.2435
	6289	5.3	Mg II 2803 Å	>1.2435
3FGLJ0930.7+5133	4678	8.9	Ca II 3934 Å	0.1893
	4720	6.9	Ca II 3968 Å	0.1893
	5119	4.1	*G*-band 4305 Å	0.1893
	5955	1.4	[O III] 5007 Å	0.1893
	6155	2.1	Mg I 5175 Å	0.1893
	7008	1.2	Na I 5892 Å	0.1893
3FGLJ1146.1-0640	6454	2.2	Ca II 3934 Å	0.6407
	6511	3.2	Ca II 3968 Å	0.6407
	6730	0.8	H_δ 4102 Å	0.6407
	7062	1.5	*G*-band 4305 Å	0.6407
3FGLJ1223.3+0818	4805	0.5	Mg II 2796 Å	>0.7187
	4818	0.4	Mg II 2803 Å	>0.7187
3FGLJ1234.7-0437	4373	7.7	[Ne V] 3426 Å	0.2765
	4756	18.1	[O II] 3727 Å	0.277
	4938	7.4	[Ne III] 3869 Å	0.2765
	5023	3.1	Ca II 3934 Å	0.277
	5068	5.6	Ca II 3968 Å	0.277
	5497	1.2	*G*-band 4305 Å	0.2775
	6205	7.0	H_β 4861 Å	0.2765
	6328	11.4	[O III] 4959 Å	0.2765
	6391	28.7	[O III] 5007 Å	0.2765
	6605	2.5	Mg I 5175 Å	0.2765
	6727	1.4	Ca+Fe 5269 Å	0.2765
	7522	3.0	Na I 5892 Å	0.2765
3FGLJ1258.4+2123	6398	3.2	Ca II 3934 Å	0.6265
	6455	4.8	Ca II 3968 Å	0.6265
	7001	2.3	*G*-band 4305 Å	0.6265
3FGLJ1541.6+1414	4811	1.2	Ca II 3934 Å	0.223
	4853	1.2	Ca II 3968 Å	0.223
	6123	1.1	[O III] 5007 Å	0.223
3FGLJ2150.5-1754	4663	3.8	Ca II 3934 Å	0.1855
	4704	3.6	Ca II 3968 Å	0.1855
	5103	1.4	*G*-band 4305 Å	0.1855
	5765[a]	0.9	H_β 4861 Å	0.1855
	6135	1.3	Mg I 5175 Å	0.1855
	6986	1.4	Na I 5892 Å	0.1855

Table 4
(Continued)

Object name	λ	EW	Line ID	z
3FGLJ2209.8-0450	5204	0.9	[O II] 3727 Å	0.3967
	5495	1.3	Ca II 3934 Å	0.3967
	5543	1.7	Ca II 3968 Å	0.3967
	6012	1.0	*G*-band 4305 Å	0.3967
3FGLJ2212.5+0703	5600	116	Mg II 2800 Å	1.00
3FGLJ2228.5-1636	~6020	···	Ca II break	~0.525
3FGLJ2229.1+2255	5664	0.8	Ca II 3934 Å	0.440
	5715	1.0	Ca II 3968 Å	0.440
	6198	1.1	*G*-band 4305 Å	0.440
3FGLJ2244.6+2503	6491[a]	0.5	Ca II 3934 Å	0.650
	6548	0.4	Ca II 3968 Å	0.650
3FGLJ2246.2+1547	5949	1.6	[O II] 3727 Å	0.5965
	6280[a]	1.5	Ca II 3934 Å	0.5965
	6336[a]	0.8	Ca II 3968 Å	0.5965
3FGLJ2250.3+1747	4604	2.5	[Ne V] 3426 Å	0.3437
	5008	3.5	[O II] 3727 Å	0.344
	5286	7.6	Ca II 3934 Å	0.3437
	5332	9.0	Ca II 3968 Å	0.3437
	5512	1.3	H_δ 4102 Å	0.3437
	5784	1.7	*G*-band 4305 Å	0.3437
	5833	0.8	H_γ 4340 Å	0.3437
	6663	2.1	[O III] 4959 Å	0.3437
	6728	6.5	[O III] 5007 Å	0.3437
3FGLJ2321.6-1619	6663	0.5	Ca II 3934 Å	0.6938
	6722	0.3	Ca II 3968 Å	0.6938
3FGLJ2358.5+3827	4472	11.4	[O II] 3727 Å	0.2001
	4642	1.3	[Ne III] 3869 Å	0.2000
	4721	0.8	Ca II 3934 Å	0.2001
	5166	1.1	*G*-band 4305 Å	0.2001
	5209	1.0	H_γ 4340 Å	0.2001
	5834	2.7	H_β 4861 Å	0.2001
	5951	4.9	[O III] 4959 Å	0.2001
	6009	16.2	[O III] 5007 Å	0.2001
	6211	1.1	Mg I 5175 Å	0.2001
	7072	1.7	Na I 5892 Å	0.2001

Note. Column 1: name of the target; Column 2: barycenter of the detected line; Column 3: measured equivalent width; Column 4: line identification; Column 5: spectroscopic redshift.
[a] The marker indicates that the line is partially contaminated by telluric band.

In our spectrum, a faint emission line is clearly detected at 7278 Å which we attribute to [O III] 5007 Å at $z = 0.4537$, since another weaker emission line corresponding to [O III] 4959 Å is also present (although it is partially contaminated by telluric absorption).

3FGL J0234.2-0629. Through the *Swift*/XRT data analysis, we found only one X-ray source (XRT J023410-062829) inside the 3FGL position error box. We propose the spatially coincident object SDSS J023410.30-062825.7 ($g = 20.5$) as the likely optical counterpart.

Our spectrum exhibits a typical power law of the continuum and a strong (EW = 6.9 Å) absorption feature is detected at 4564 Å which we interpret as an intervening absorption system due to Mg II 2800 Å at $z = 0.63$. This represents the spectroscopic redshift lower limit of the target. No other emission or absorption lines are detected. Recently an optical spectrum was

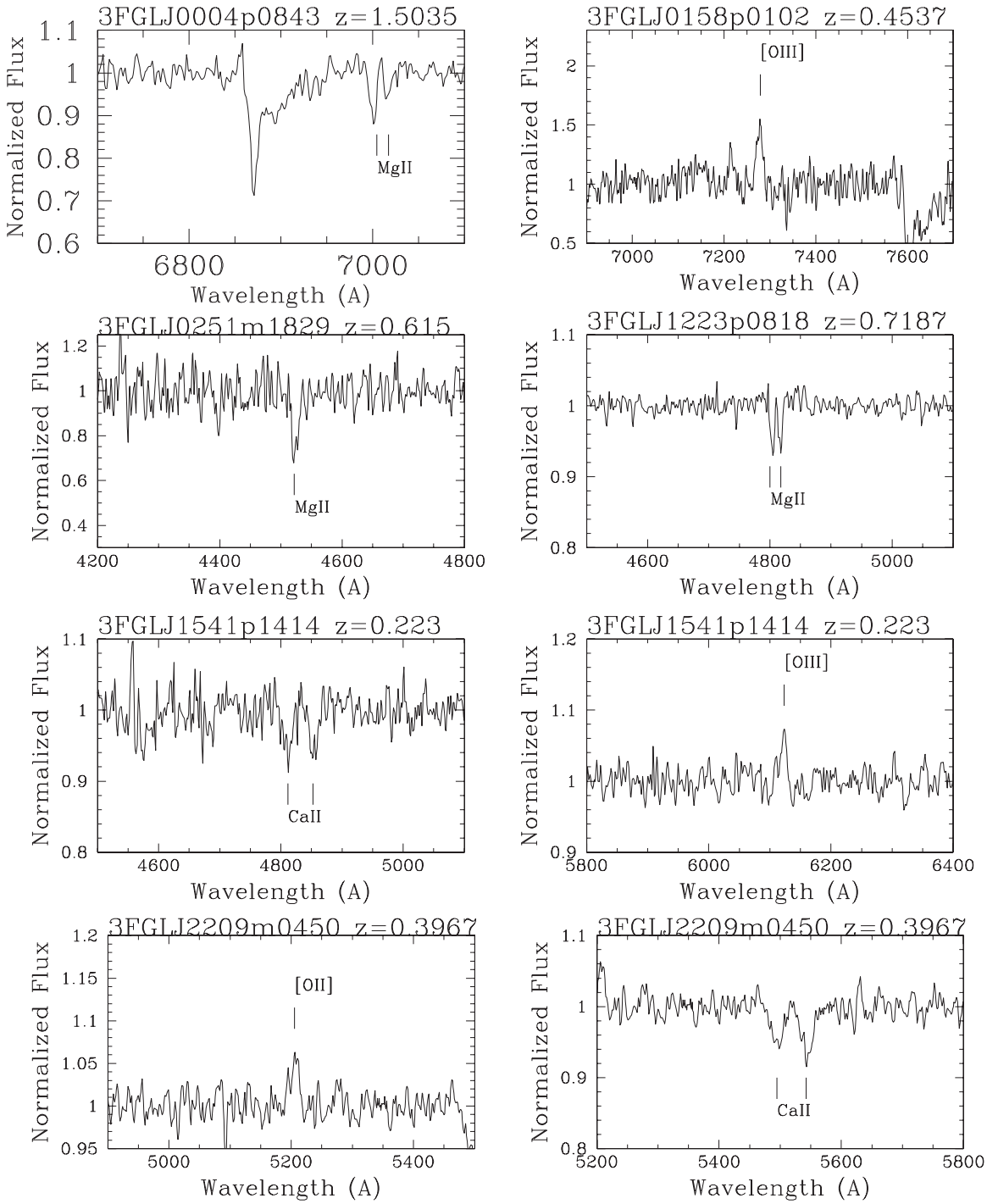

Figure 3. Close-ups of the normalized spectra around the faintest detected spectral features of the UGSs obtained at the GTC. Main telluric bands are indicated as ⊕, spectral lines are marked by line identification.

obtained by the SDSS, but no indication of redshift was given, although the intervening absorption is clearly detected.

3FGLJ0251.1-1829. This UGS is also reported in the 3FHL catalog. From the *Swift*/XRT data analysis, we reveal an X-ray source (XRT J025111-183141) inside the γ-ray error box, which is positionally coincident with the radio source NVSS J025111-183112 and the optical counterpart USNOB1-0714-0029276. No previous optical spectra, classification, or redshift are in the literature.

We observed this source at magnitude $g = 19.1$, under modest sky conditions. Our spectrum is dominated by non-thermal power-law emission supporting the BLL nature of this target. A narrow absorption feature is detected at $\sim$4522 Å which we attribute as due to the Mg II 2800 Å intervening system and set a spectroscopic redshift lower limit of the target of $z > 0.615$.

3FGLJ0258.9+0552. The possible X-ray counterpart (XRT J025857+055243) of this 3FHL source is found from

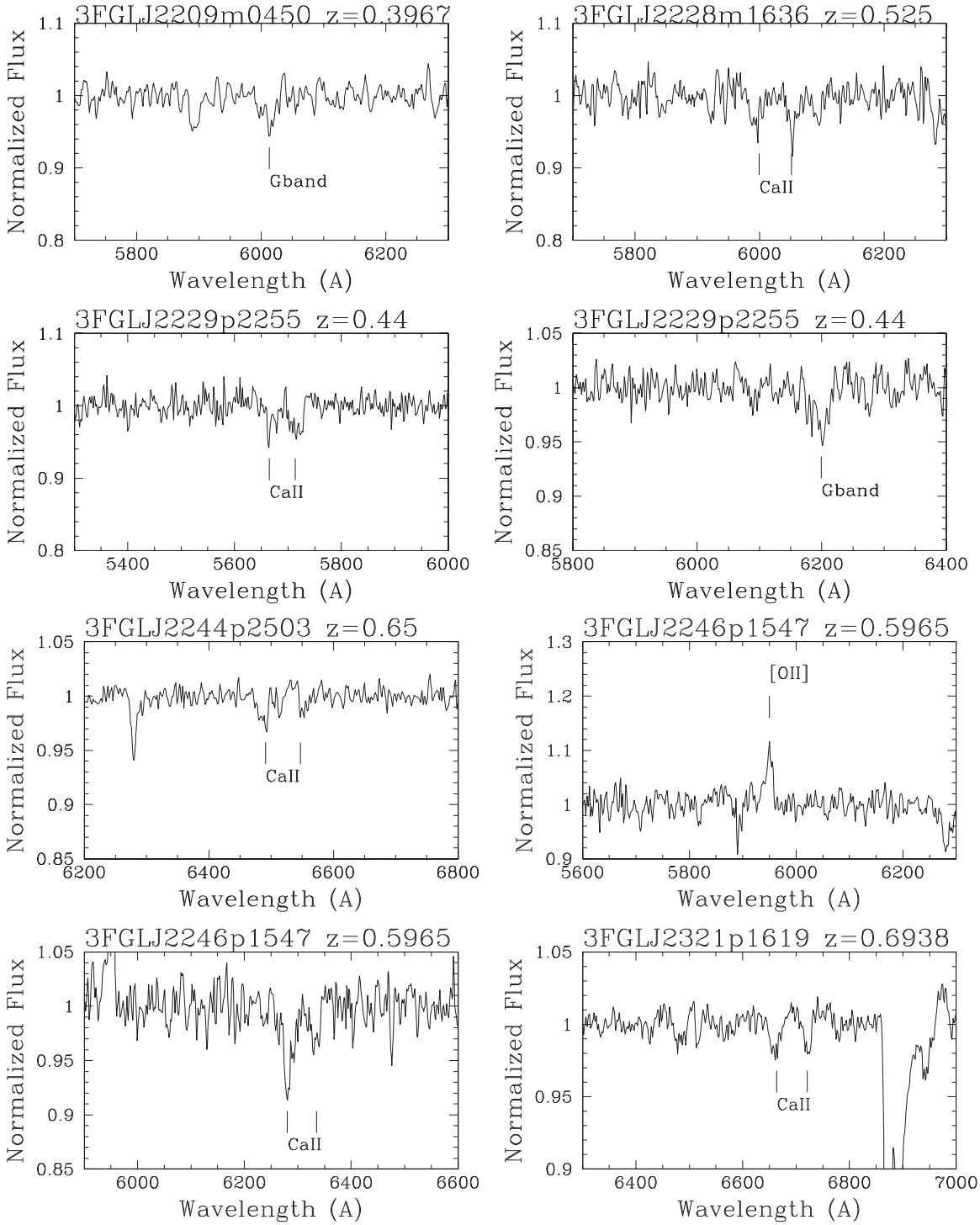

Figure 3. (Continued.)

the *Swift*/XRT analysis. We propose SDSS J025857.55 +055243.9 as the optical counterpart, coincident also with the UV and radio sources GALEXASC J025857.49 +055244.3 and 1WGA J0258.9+0552. No information about the nature and the redshift of the source is published in the literature.

Our spectrum is featureless and clearly indicates a BLL classification of the target. Several features, visible in the bluer part of the spectrum, are consistent with diffuse interstellar band absorptions. Under the assumption of an elliptical host galaxy for the BLL, we can set a lower limit of the redshift $z > 0.7$ based on the minimum EW of absorption features expected from the host galaxy (details in Paiano et al. 2017b).

3FGLJ0414.9-0840. The X-ray counterpart is XRT J041433-084208 and in the optical is coincident with USNOB1-0812-0041101 and the radio source NVSS J041433-084206.

Our optical spectrum classifies the target as a BLL because of the featureless power-law continuum. Recently another optical spectrum of the target, presented by Peña-Herazo et al. (2017), has confirmed our classification. As no emission or

absorption lines are detected, the redshift of this target remains unknown. We can set a lower limit of $z > 0.35$ based on the non-detection of the absorption features from the starlight of the elliptical host galaxy (details in Paiano et al. 2017b).

3FGLJ0506.9+0321. For this 3FHL UGS, we found only the X-ray source XRT J050650+032358 inside the *Fermi* error-box, and the optical counterpart is USNOB1-0933-0085213, coincident with the UV object GALEXASC J050650.15+032358.7 and radio source NVSS J050650+032401. No previous optical spectra are available in the literature.

Our spectrum shows a featureless shape, typical of the BLL, and the redshift remains unknown. We set a lower limit of $z > 0.1$ according to the method outlined in Paiano et al. (2017b), based on the lack of stellar features of the host galaxy and on the measure of the minimum EW.

3FGLJ0848.5+7018. Inside the positional γ-ray error box of this 3FHL object, we found only one radio counterpart NVSS J084839+701727 and we propose as an optical association the object USNOB1-1602-0082223, coincident with the radio and UV objects 87GB 084343.8+702846 and GALEXASC J084839.45+701726.8.

Our optical spectrum is characterized by a continuum emission which establishes the identification as a BLL. No significant emission lines are apparent, but we clearly detect three absorption line systems (see also Table 4) at ∼5344 Å and ∼5833 Å, which we identified as intervening features due to Fe II 2382, 2600 Å, and at ∼6280 Å attributed to Mg II 2800 Å at $z = 1.2435$. Therefore this value represents the spectroscopic redshift lower limit of the target. A similar case was found in our first data set in Paper I for the source 3FGL J1129+3705.

3FGLJ0930.7+5133. The X-ray counterpart for this UGS, found by the *Swift*/XRT analysis, is XRT J093033+513211. It coincides with the radio source NVSS J093033+513216 and in the optical with SDSS J093033.27+513214.5. No previous optical spectra are found in the literature.

In our optical spectrum, we are able to detect absorption lines (see Table 4) due to Ca II 3934, 3968 Å, *G*-band 3405 Å, Mg I 5175 Å, and Na I 5892 Å, typical of the elliptical host galaxy, and a weak emission line at ∼5955Å due to [O III] 5007 Å that sets the source at $z = 0.1893$.

3FGLJ1146.1-0640. This target is a hard γ-ray object present also in the 3FHL catalog. XRT J114600-063855 is the only X-ray source detected inside the *Fermi* position error box and it is coincident with the UV source GALEXASC J114600.86-063854.6 and the optical object USNOB1-0833-0250645.

In our spectrum, the continuum is very flat ($\alpha = -0.25$) and no emission lines are present, but we are able to detect absorption lines identified as the Ca II 3934, 3968 Å, H_δ, *G*-band 4305 Å, and H_γ, due to the stellar emission of the host galaxy at $z = 0.6407$.

3FGLJ1223.3+0818. We obtain the optical spectrum of the X-ray counterpart source XRT J122327+082031, likely associated with the γ-ray emitter, that establishes the BLL nature for this source. The dominant feature is an intervening absorption system at ∼4810 Å (see Table 4) due to Mg II 2800 Å at $z = 0.7187$, which is the spectroscopic redshift lower limit of the target.

3FGLJ1234.7-0437. From the *Swift*/XRT data analysis, for this 3FHL γ-ray emitter, we found only one bright X-ray source (XRT J123448-043246) within the γ-ray error box, coincident with the optical source USNOB1-0854-0232216 ($g = 18.6$) and the UV object GALEXASC J123448.20-043244.6 ($F_\nu \sim 7 \times 10^{-06}$ Jy). No radio emission is found at the position of the source. Based on a few lines from an uncalibrated optical spectrum by the 2dF Galaxy Redshift survey, a redshift of 0.277 was proposed.

Our high-quality optical spectrum clearly exhibits emission lines of [O II] 3727 Å, H_β, and [OIII] 5007 Å at $z = 0.2765$, together with stellar absorption lines of its host galaxy (see also Table 4). The emission line properties of this object are typical of Seyfert 2 galaxies.

3FGLJ1258.4+2123. We found an X-ray source XRT J125821+212350, within the 3FGL error box, that coincides with SDSS J125821.45+212351.3 ($g = 20.5$).

Our optical spectrum shows the BLL non-thermal continuum with superimposed stellar features of its host galaxy: Ca II 3934, 3968 Å at 6398 Å and 6455 Å, and the *G*-band 4305 Å at 7001 Å. Therefore the redshift of the source is $z = 0.6265$.

3FGLJ1525.8-0834. Analysis of *Swift*/XRT data reveals one X-ray object (XRT J152603-083147) in the 3FGL error box that is spatially coincident with the optical source USNOB1-0814-0287412 ($g = 18.3$), the UV object GALEXASC J152603.17-083146.0 ($F_\nu \sim 8 \times 10^{-06}$ Jy), and the radio source NVSS J152603-083146 ($F_\nu \sim 2.5 \times 10^{-01}$ Jy)).

Our optical spectrum is featureless and characterized by a power-law emission ($\alpha = -0.85$) and establishes the BLL nature. A redshift lower limit $z > 0.40$ can be set on the basis on the minimum EW method (Paiano et al. 2017b).

3FGLJ1541.6+1414. Inside the 3FGL sky region of this target, we found an X-ray source XRT J154150+141442 that is associated with the optical source SDSS J154150.09+141437.5 ($g = 18.4$). The SDSS survey provided a spectrum of the optical counterpart characterized by blue continuum emission superposed by a number of relevant absorption features: *G*-band (4305), Mg I (5175), and the weak doublet of Ca II (3934, 3968) at $z = 0.223$.

Our spectrum was obtained with a narrower slit of 1.″2, compared with that of the SDSS, and is more dominated by non-thermal emission with a relevant blue (at $\lambda < 5000$ Å) component. A weak (EW = 1.1 Å) emission line at 6123 Å attributed to [O III] 5007 Å and the absorption doublet of Ca II 3934, 3968 Å confirm the redshift $z = 0.223$.

3FGLJ2150.5-1754. Through the *Swift*/XRT data analysis, we found only one X-ray source (XRT J215046-174957) within the 3FGL error box. We propose the spatially coincident objects USNOB1-0721-1160290 ($g = 17.6$) and NVSS J215046-174954 as optical and radio counterparts.

Our optical spectrum is dominated by a galactic component with the presence of moderate non-thermal emission. Clear absorption lines of the overall stellar population are detected, in particular Ca II 3934, 3968 Å, *G*-band 4305 Å, Mg I 5157 Å, and Na I 5893 Å at $z = 0.1855$.

3FGLJ2209.8-0450. The source XRT J220941-045108 is proposed as a counterpart in the X-ray band of the target and it is associated with the radio source NVSS J220941-045111 and the optical source SDSS J220941.7-045110.2 ($g = 18.8$). There is no information about the classification and redshift in the literature.

Our optical spectrum exhibits a typical BLL continuum and is characterized by the signature of the stellar component from

the host galaxy (Ca II 3934, 3968 Å doublet, and *G*-band 4305 Å absorption) at $z = 0.3967$. In addition a weak possible emission line due to [O II] 3727 Å at 5205 Å is visible.

3FGLJ2212.5+0703. On the basis of the XRT data, we propose that the X-ray and optical counterparts of this UGS are XRT J221231+070651 and SDSS J221230.98+070652.4 ($g = 20.6$). No radio source is found as a counterpart and no previous optical spectra are present in the literature.

Our optical spectrum clearly shows a prominent and strong (EW = 116 Å) emission line at 5600 Å. If attributed to Mg II 2800 Å, the redshift is $z = 1.00$. Based on this spectrum, the target is classified as a QSO.

3FGLJ2228.5-1636. The X-ray counterpart XRT J222830-163642 is found from the *Swift*/XRT analysis. We propose as the optical counterpart USNOB1-0733-0885778, coincident with the UV source GALEXASC J222830.19-163642.7 and the radio source NVSS J222830-163643. No previous spectra or information are available in the literature for this target.

Our optical spectrum shows a power-law shape ($\alpha = -0.90$) confirming the BLL nature of the source. We note a weak signature of Ca II 3934, 3968 Å at ∼6020 Å, suggesting a tentative redshift of $z = 0.525$.

3FGLJ2229.1+2255. We found only one X-ray source (XRT J222911+225458) within the 3FGL error region of the target, which can be associated to the optical source SDSS J222911.17+225459.7 ($g = 18.9$). No radio emission is found at the position of the target.

Our optical spectrum shows characteristic non-thermal emission with weak Ca II 3934, 3968 Å and *G*-band 4305 Å absorption lines (see Table 4 and Figure 3) at $z = 0.440$.

3FGLJ2244.6+2503. From the XRT analysis, we detect the source XRT J224436+250343 inside the γ-ray error box coincident with radio and optical objects NVSS J224436 +250345 and SDSS J224436.70+250342.6. An optical spectrum was recently provided by the SDSS that appears featureless.

We obtained a good (S/N ∼ 120) optical spectrum characterized by a power-law continuum with spectral index $\alpha = -1.0$. This supports the BLL classification for the source. Two weak absorption features are detected at ∼6500Å, partially contaminated by a small telluric absorption. They are consistent with the Ca II 3934, 3968 Å absorption doublet at $z = 0.650$. No other absorption or emission lines are found at this redshift. We consider this redshift as tentative.

3FGLJ2246.2+1547. This source is associated with the radio source NVSS J224604+154437 and the optical source SDSS J224604.99+154435.3. This source was present in our first data set Paper I and was classified as a BLL on the basis of the optical spectrum that appeared without evident emission/absorption lines.

The source was re-observed in August 2017 with a better grism resolution and the new spectrum (see Figure 3) reveals an emission line (EW = 1.6 Å) at 5949 Å identified as due to [O II] 3727 Å at $z = 0.5965$. Also a weak absorption doublet at ∼6300 Å, which we identified as Ca II 3934, 3968 Å at the same redshift, is present although it is contaminated by telluric absorption.

3FGLJ2250.3+1747. We obtained the optical spectrum of the source SDSS J225032.7+174914.9, coincident with the only X-ray counterpart XRT J225031+124916 found inside its γ-ray error position. This coincides also with the radio source NVSS J225032+174914.

The spectrum is characterized by several features due to the host galaxy. In particular we detect absorption lines due to Ca II 3934, 3968 Å, H_δ, *G*-band 4305 Å, H_γ, and H_β, together with emission lines attributed to Ne V 3426 Å, [O II] 3727 Å, and [O III] 4959, 5007 Å (see Table 4). Therefore, the redshift of the source is $z = 0.3437$.

3FGLJ2321.6-1619. We propose the source XRT J232136-161926 as the X-ray counterpart for this UGS, coincident with the optical object USNOB1-0736-0835813 ($g = 16.9$) and the radio NVSS J232137-161935. No previous optical spectra are found in the literature and its classification remains uncertain.

Our spectrum establishes the BLL nature of the source and exhibits the characteristic power-law continuum ($\alpha = -1.15$). We detect the absorption doublet attributed to Ca II 3934, 3968 Å at 6663 Å and 6722 Å, which locates the source at $z = 0.6938$.

3FGLJ2358.6-1809. XRT J235836-180718 is the only *Swift* source detected inside the 3FGL position error of the target and is considered the X-ray counterpart. It is associated with the optical object USNOB1-0718-1032041 ($g = 17.7$) and the radio NVSS J235836-180718. On the basis of an optical spectrum secured by the 6dF Survey, a redshift of $z = 0.0575$ was proposed. However, no clear features are visible in that spectrum and the redshift is dubious.

Our optical spectrum (S/N = 130) appears featureless, establishing the BLL nature of this source. Based on the assumption of the typical BLL host galaxy being a giant elliptical galaxy, by the minimum EW method outlined in Paiano et al. (2017b), we can set a lower limit of the redshift of > 0.25.

3FGLJ2358.5+3827. The source is classified as a UGS also in the 3FHL catalog. Inside the *Fermi* error box there is only one X-ray source (XRT J235825+382857) and the radio source (NVSS J235825+382857), which also coincides with the optical object USNOB1-1284-0547072 ($g = 18.4$). No optical spectra of this object are available in the literature.

Our optical spectrum shows a number of narrow emission lines of [O II] 3727 Å, [Ne III] 3869 Å, H_β, and [O III] 4959, 5007 Å and the typical absorption features due to the stellar population of its host galaxy (see Table 4), yielding the redshift $z = 0.2001$. The emission line properties of this object are typical of Seyfert 2 galaxies.

5. Conclusions

We secured optical spectroscopy of 28 UGSs that, together with other 20 sources previously investigated (Paper I), led to almost complete (at 80% level) the optical investigation of the sample of unidentified γ-ray sources defined in Paper I. This allows us to characterize and to classify all these sources, and to measure the redshift for most of them.

From the analysis of the spectroscopic properties of all observed targets (47 out of 60), we find that:

1. all targets exhibit an AGN optical spectrum: 44 are classified as BLLs, one is a QSO, two objects have a Seyfert 2 type spectrum, and in one case the source is classified as an NLSy1;

2. for 39 objects we measure their spectroscopic redshift: 29 sources exhibit emission and/or absorptions lines, allowing us a firm measurement of the redshift, while for 10 objects we set a spectroscopic lower limit of the redshift on the basis of the detection of absorption lines from intervening systems due to Mg II 2800 Å and/or Fe II 2382, 2600 Å.

The redshift range of our UGS data set spans from $z = 0.171$ up to $z = 0.787$. The averaged value is $\langle z \rangle = 0.45$. For the 10 objects with a spectroscopic lower limit, the range is between 0.38 and 1.5. We note that the source 3FGL J0004.2+0843, which is found at $z > 1.5035$, is among the farthest BLLs known detected by the *Fermi* satellite (see also Paiano et al. 2017c) and it is one of the few BLLs known at $z > 1$.

Although the optical spectroscopy confirms that the majority of the sources (∼90%) are blazars (as expected), in three cases their spectra indicate a different classification. In particular, the source 3FGL J0031.6+0938, showing a broad component of the H_β emission line, can be classified as an NLSy1 and takes to six the total number of known objects that are classified as NLSy1 in the 3FGL catalog. The other two sources that are not classified as blazars show an optical spectrum typical of Seyfert 2 galaxies with only narrow emission lines. It is worth noting that in the current *Fermi* catalog there are only two other sources that exhibit a Seyfert 2 optical spectrum (Lenain et al. 2010; Ackermann et al. 2012). The latter (NGC 1068 and NGC 4945) are at much lower redshift ($z = 0.0038$ and $z = 0.0019$, respectively) with respect to the redshift ($z \sim 0.2$–0.3) of the Seyfert 2-type sources found in this work.

Only nine sources in our sample have a featureless optical spectrum and for them we set redshift lower limits (see Table 3 of this work and Paper I), based on the minimum detectable EW technique and on the lack of detection of host galaxy absorption lines, assuming a BLL host galaxy with $M(R) = -22.9$ (see the details in Paiano et al. 2017b).

Finally, we note that 25 targets of our whole sample are also reported in the 3FHL catalog, included the two Seyfert 2-like sources and 16 BLLs with a measurement of the redshift (five with high redshift >0.5); therefore they can be considered as interesting targets for future observations with the next-generation TeV Cherenkov telescopes.

We acknowledge the anonymous referee for constructive suggestions and comments that allowed us to improve our paper.

We acknowledge support from INAF under PRIN SKA/CTA ''FORECaST.'' The financial contribution by the contract *Studio e Simulazioni di Osservazioni (Immagini e Spettri) con MICADO per E-ELT* (DD 27/2016—Ob. Fun. 1.05.02.17) of the INAF project *Micado simulazioni casi scientifici* is acknowledged.

Facilities: GTC-OSIRIS, (Cepa et al. 2003).

Software: IRAF (Tody 1986, 1993).

ORCID iDs

Simona Paiano https://orcid.org/0000-0002-2239-3373
Renato Falomo https://orcid.org/0000-0003-4137-6541
Aldo Treves https://orcid.org/0000-0002-0653-6207
Riccardo Scarpa https://orcid.org/0000-0001-9118-8739

References

Acero, F., Ackermann, M., Ajello, M., et al. 2015, ApJS, 218, 23
Acero, F., Donato, D., Ojha, R., et al. 2013, ApJ, 779, 133
Ackermann, M., Ajello, M., Allafort, A., et al. 2012, ApJ, 755, 164
Atwood, W. B., Abdo, A. A., Ackermann, M., et al. 2009, ApJ, 697, 1071
Cardelli, J. A., Clayton, G. C., & Mathis, J. S. 1989, ApJ, 345, 245
Cepa, J., Aguiar-Gonzalez, M., Bland-Hawthorn, J., et al. 2003, Proc. SPIE, 4841, 1739
D'Abrusco, R., Massaro, F., Paggi, A., et al. 2013, ApJS, 206, 12
Doert, M., & Errando, M. 2014, ApJ, 782, 41
Falomo, R., Pian, E., & Treves, A. 2014, A&ARv, 22, 73
Garofalo, D., Singh, C. B., Walsh, D. T., et al. 2018, arXiv:1809.00724
Komossa, S. 2008, RMxAC, 27, 86
Landi, R., Bassani, L., Stephen, J. B., et al. 2015, A&A, 581, A57
Lenain, J.-P., Ricci, C., Türler, M., Dorner, D., & Walter, R. 2010, A&A, 524, A72
Massaro, F., D'Abrusco, R., Tosti, G., et al. 2012, ApJ, 752, 61
Massaro, F., Masetti, N., D'Abrusco, R., Paggi, A., & Funk, S. 2014, AJ, 148, 66
Mirabal, N., Frías-Martinez, V., Hassan, T., & Frías-Martinez, E. 2012, MNRAS, 424, L64
Padovani, P., Alexander, D. M., Assef, R. J., et al. 2017, A&ARv, 25, 2
Paiano, S., Falomo, R., Franceschini, A., Treves, A., & Scarpa, R. 2017a, ApJ, 851, 135
Paiano, S., Landoni, M., Falomo, R., et al. 2017b, ApJ, 837, 144
Paiano, S., Landoni, M., Falomo, R., Treves, A., & Scarpa, R. 2017c, ApJ, 844, 120
Peña-Herazo, H. A., Marchesini, E. J., Álvarez Crespo, N., et al. 2017, Ap&SS, 362, 228
The Fermi-LAT Collaboration 2017, arXiv:1702.00664
Tody, D. 1986, Proc. SPIE, 627, 733
Tody, D. 1993, in ASP Conf. Ser. 52, Astronomical Data Analysis Software and Systems II, ed. R. J. Hanisch, R. J. V. Brissenden, & J. Barnes (San Francisco, CA: ASP), 173